

A Deeper Investigation of the Primordial Binary Cluster Candidate

QINGSHUN HU,¹ SONGMEI QIN,^{2,3,4} CHUNYAN LI,¹ CHENGLONG LV,⁵ YANG PAN,¹ AND YANGPING LUO¹

¹*School of Physics and Astronomy, China West Normal University, No. 1 Shida Road, Nanchong 637002, People's Republic of China*

²*Institut de Ciències del Cosmos, Universitat de Barcelona (ICCUB), Martí i Franquès 1, 08028 Barcelona, Spain*

³*Key Laboratory for Research in Galaxies and Cosmology, Shanghai Astronomical Observatory, Chinese Academy of Sciences, 80 Nandan Road, Shanghai 200030, People's Republic of China*

⁴*School of Astronomy and Space Science, University of Chinese Academy of Sciences, No. 19A, Yuquan Road, Beijing 100049, People's Republic of China*

⁵*Xinjiang Astronomical Observatory, Chinese Academy of Sciences, No. 150, Science 1 Street, Urumqi, Xinjiang 830011, People's Republic of China*

ABSTRACT

We hereby reported a new physical binary cluster (ASCC 19 and ASCC 21) near the Orion star-forming complex based on the data in the literature. Analysis of the results shows that it is a primordial binary cluster. It is possible that this binary cluster is undergoing two-body relaxation by inspecting the radial velocity anomalies of its member stars. In addition, based on the analysis of its metal abundances, we found that the components of this binary cluster may have been formed by the deep fusion of multiple subclusters. Finally, we investigated the 3D morphology of this binary cluster, simulated the trajectories of its components in the galactic disk, and concluded that its components may not merge into a single cluster.

Keywords: Galaxy: stellar content — open cluster: ASCC 19 and ASCC 21

1. INTRODUCTION

Open clusters (OCs) that form in the giant molecular clouds are an important part of composing the Milky Way (Lada & Lada 2003). Most of them all survive in isolation in the galactic disk. However they also live in the Galactic disk as binary, triple, and multiple clusters (e.g. Song et al. 2022; Qin et al. 2023) whose proportion is almost comparable to that, about 10% (Bhatia & Hatzidimitriou 1988; Hatzidimitriou & Bhatia 1990) or 12% (Pietrzynski & Udalski 2000), of pairs in the Magellanic Cloud (de La Fuente Marcos & de La Fuente Marcos 2009). The results obtained by (de La Fuente Marcos & de La Fuente Marcos 2009) show that most known binary clusters have very young components (young OCs). Therefore, they are ideal objects used to study and understand the formation and evolution of OCs.

There are several formation channels used to explain the existence of pairs, triplets, or higher multiplicity clusters. First, binary clusters can be formed by tidal capture (van den Bergh 1996). These pairs, not primordial OC binaries, usually share a common motion veloc-

ity, with different chemical compositions and ages. Second, the resonances of the non-axisymmetric component of the Galactic potential, typically induced by the Galactic bar or spiral arms (e.g. Dehnen 1998; De Simone et al. 2004; Famaey et al. 2005; Chakrabarty 2007), can also result in the formation of double clusters. Third, cluster pairs formed in the same giant molecular cloud at the same time. In this case, they are expected to have similar ages, kinematic characteristics, and chemical composition. The scenario is similar to the simultaneous or primordial formation Fujimoto & Kumai (1997) and Bekki et al. (2004) have elucidated. Finally, double clusters also formed in the sequential formation of OCs. It is well known that supernova shocks or massive stellar winds in one cluster may result in the other one formation out of nearby clouds, then generate a cluster pair (Brown et al. 1995; Goodwin 1997).

There has been a lot of work on the discovery of binary clusters. For example, Pavlovskaya & Filippova (1989) and (Subramaniam et al. 1995) identified 5 possible cluster groups and 18 possible cluster pairs, respectively. After that, de La Fuente Marcos & de La Fuente Marcos (2009) found 34 OC pairs based on the OC samples from NCOVOC (Dias et al. 2002) and WEBDA (Mermilliod & Paunzen 2003). Conrad et al.

(2017) discovered 14 binary clusters from the catalogue provided by Kharchenko et al. (2004, 2005). Recently, Song et al. (2022) and Li & Zhu (2024) found 14 candidates of truly binary OCs based on the catalog data from Cantat-Gaudin et al. (2020) and 13 newly close binary OCs using the OC catalog of Hunt & Reffert (2023) that were obtained based on Gaia data, respectively. Similarly, Casado (2021) identified 22 new binary or multiple OCs from the catalogs of OCs (Kharchenko et al. 2013; Cantat-Gaudin et al. 2018, 2020; Bica et al. 2019; Liu & Pang 2019; Sim et al. 2019; Castro-Ginard et al. 2020). Then, they (Casado 2021) also found a new binary OC, named Casado 9 and Casado 10, by using Gaia DR2.

Nevertheless, there are many works that reported a set number of new binary OCs, it can still be expected that there are many more new binary clusters in the Milky Way, especially the discovery of primordial binary OCs. The primordial binary OCs may be the final products of multiple mergers of some smaller clusters or stellar groups (de La Fuente Marcos & de La Fuente Marcos 2009). Meanwhile, they also may be potential binary cluster candidates to be merged. Thanks to the precision of Gaia data, there is an opportunity that lets us discover new primordial binary OCs from a newly published catalog of OCs (van Groenigen et al. 2023) taking from the third Gaia Data Release (Gaia DR3) (Gaia Collaboration et al. 2023). With this aim, we searched for all nearby OCs from the OCs catalog published by van Groenigen et al. (2023). We indeed discovered a new primordial OC pair (ASCC 19 and ASCC 21), which was not reported in previous works. The rest of this article is structured as follows: Sect. 2 describes how we selected the data; Sect. 3 presents the results of the primordial OC pair; a summary is presented in Sect. 4.

2. DATA SELECTION

The member stars of ASCC 19 and ASCC 21 were taken from a members' catalog of 2492 OCs published by van Groenigen et al. (2023) on Gaia DR3 data that was obtained by a deep neural network architecture method on the parameter reference of OCs catalog from Cantat-Gaudin et al. (2020) and Castro-Ginard et al. (2022). This catalog has the advantage of providing, as far as possible, the more complete member stars of OCs, since it contains many faint stars (see their Fig. 4), which were not in the previous catalogs. In their catalog, we found that ASCC 19 and ASCC 21 included 3861 and 2709 members, respectively, which are given in Table. 1. The membership probabilities of both member lists are ranging from 0 to 1. In the present study, in order to ensure the reliability of the results, we filtered out those members with a probability of less than 1. Therefore,

there are 1250 members in ASCC 19 and 998 members in ASCC 21 we obtained where these stars can be regarded as truly members.

3. RESULTS

3.1. Primordial Binary Cluster

The simulations conducted by Bekki et al. (2004) suggested that binary star clusters can be formed in cloud-cloud collisions. Initially, when two clouds collide, the intense compression and dissipation of gas will form an elongated molecular cloud. After that, two dense clusters will be formed in the high-density region of the two clouds. As the orbital angular momentum of the two molecular clouds will be transferred to the two clusters, they will begin to evolve around each other (Bekki et al. 2004, see their Fig. 2). If the two molecular clouds have the same properties, such as metal abundance, Then the binary cluster can be regarded as a primordial binary cluster.

In the present work, we discovered a primordial binary cluster (ASCC 19 and ASCC 21) from literature (van Groenigen et al. 2023). Figure 1 shows the member distributions of ASCC 19 and ASCC 21 in a 2D celestial coordinate system, parallax, proper motion, and CMD spaces. We can see from the figure that ASCC 19 and ASCC 21 are a truly physical binary cluster because their spatial position is very close to each other, with their proper motion being similar, even their ages. The related parameters of the cluster pair are listed in Table 1, which also indicates the double cluster is real and reliable. Due to the proximity and overlap of the two clusters, we performed the crossmatch of the member stars of the two clusters. What we found interesting is that there are 191 member stars from both clusters in the cross-matches. In other words, they belong to both ASCC19 and ASCC21. This may mean that the binary cluster is merging.

In order to determine whether the binary cluster we found is a primordial binary cluster, we should also check their radial velocities (Rv) in addition to checking their ages. Therefore, we plotted the histogram of the radial velocities of these two clusters, as shown in Fig. 2. The histogram was based on the removal of unreliable radial velocities, due to the ratio of the radial velocity with its error less than 3. Figure. 2 presents the rectangular distribution of the radial velocity of the double star cluster, which shows the characteristics of centralization and dispersion on both sides. Based on this, we can calculate the median of radial velocity and its error for the two clusters, respectively. The distribution over a range of 3 times the median error of the radial velocity is demonstrated within both red boxes in Fig. 2.

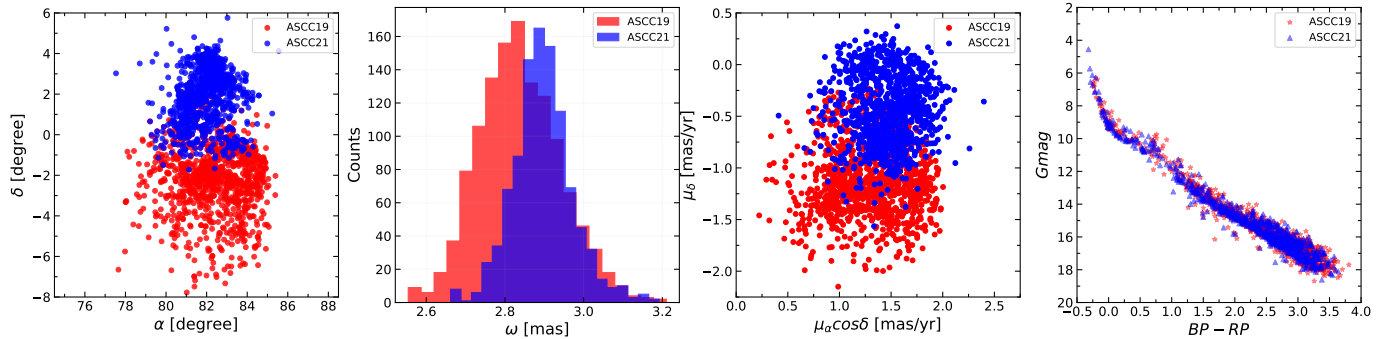


Figure 1. Member distributions of ASCC 19 and ASCC 21 in multi-dimensional parameter space. All members have a membership probability equal to 1. The members of ASCC 19 are marked by red dots or pentagams, with the members of ASCC 21 being represented by blue dots or triangles. Leftmost panel: member distribution of both clusters in a two-dimensional (2D) celestial coordinate system. Middle left panel: histograms of the member stars of both clusters in parallax space. Middle right panel: member distribution of both clusters in proper motion space. Rightmost panel: Color Magnitude Diagram (CMD) of the two clusters. It should be noted that all member data is taken from [van Groenigen et al. \(2023\)](#).

Table 1. Overall parameters of the binary clusters

Parameters	Description	ASCC 19	ASCC 21
α (degree)	Right ascension	82.31 ± 1.07	81.91 ± 0.68
δ (degree)	Declination	-1.89 ± 1.04	1.91 ± 0.96
μ_α (mas \cdot yr $^{-1}$)	Proper motion in right ascension	1.34 ± 0.25	1.48 ± 0.17
$\mu_\delta \cos \alpha$ (mas \cdot yr $^{-1}$)	Proper motion in declination	-1.12 ± 0.24	-0.44 ± 0.28
ω (mas)	Parallax	2.83 ± 0.07	2.89 ± 0.04
Rv (km \cdot s $^{-1}$)	The radial velocity	21.34 ± 4.47	20.05 ± 3.86
[Fe/H] (dex)	The metal abundance	-0.37 ± 0.15	-0.35 ± 0.21
Number of all members (-)	the number of members	3861	2709
Number of real members (-)	the number of members with Pmemb = 1	1250	998
X (pc)	The space position along X axis	-301.70 ± 5.42	-306.73 ± 3.48
Y (pc)	The space position along Y axis	-140.17 ± 6.90	-118.23 ± 4.11
Z (pc)	The space position along Z axis	-114.59 ± 5.76	-103.93 ± 5.15

On the contrary, the member stars not in the two red boxes can be regarded as outlier member stars, especially those with radial velocities above $100 \text{ km}\cdot\text{s}^{-1}$. In the next subsection, we conducted an analysis of these outlier member stars.

3.2. Outlier Member Analysis

As those outlier members on the radial velocity parameter are also truly member stars of our cluster pair ([Hu et al. 2022](#)), and they may shed important information on the evolution of the binary cluster, it is necessary to explore them in detail. Figure 3 shows the distribution of member stars in our binary cluster with a ratio of the radial velocity to its error greater than or equal to 3 in four different parameter spaces. Similar to Fig. 1, we still found an overlap of members with radial velocity in the position, parallax, proper motion, and CMD spaces. Moreover, it is apparent in paral-

lax space that the spatial distribution of those outlier member stars runs through the entire internal structure of this binary cluster. Meanwhile, interestingly, most of these outlier member stars are faint stars, which can also be seen as less massive, as shown in the rightmost panel of Fig. 3. Since the outlier member stars have relatively large radial velocities, this may indicate that the two-body relaxation process (e.g., [Bergond et al. 2001](#); [Ryon et al. 2017](#); [Mamon et al. 2019](#)) is underway within the binary cluster. The two-body relaxation leads to the less massive member stars gaining more kinetic energy and gradually moving to the outskirts of clusters, while the more massive member stars lose kinetic energy and thus sink to the center of clusters. Eventually, it may show a mass segregation phenomenon (e.g., [Vesperini et al. 2009](#); [Portegies Zwart et al. 2010](#); [Evans & Oh 2022](#); [Noormohammadi et al. 2023](#)).

Table 2. The parameters of outlier members with abnormal radial velocity

(1)	(2)	(3)	(4)	(5)	(6)	(7)	(8)	(9)
Gaia DR3 ID	Ra	Dec	Parallax	Rv	[Fe/H]	TIC ID	Host cluster	Color in Table 3
–	(degree)	(degree)	(mas)	(km/s)	(dex)	–	–	–
3220751346266572672	83.14	-0.41	2.842	-126.77 ± 5.71	-0.521	50788524	ASCC 19 and ASCC 21	Red pentagram
3223872069503741568	82.30	2.89	2.912	117.98 ± 7.80	-0.260	264682835	ASCC 19 and ASCC 21	Blue pentagram
3217579220861913472	84.04	-1.36	2.835	114.34 ± 7.75	-0.414	427451326	ASCC 19	Purple pentagram
3210550073087799296	82.17	-4.22	2.928	122.30 ± 6.34	-0.136	50587538	ASCC 19	Pink pentagram
3234192596742088192	80.65	1.70	2.934	107.20 ± 6.97	–	–	ASCC 21	Black pentagram
3223841450681464448	82.43	2.55	2.948	137.78 ± 5.76	–	264739961	ASCC 21	Coral pentagram
3220123147170971520	82.05	-1.77	2.899	17.73 ± 3.96	-4.096	–	ASCC 19	Orange pentagram
3217595988412324352	83.98	-1.23	2.937	-36.07 ± 6.84	-2.991	427399934	ASCC 19	Cyan pentagram

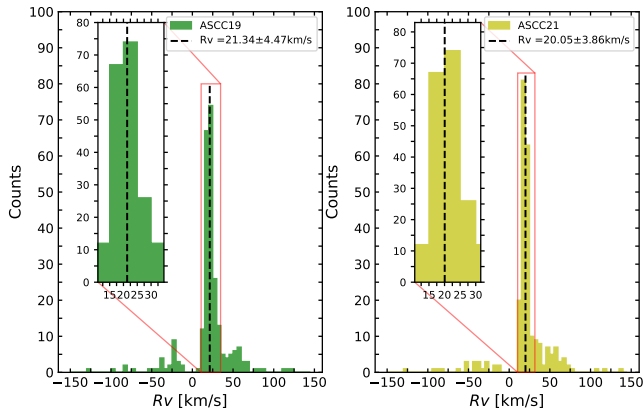


Figure 2. Left panel: radial velocity histogram of ASCC 19. Right panel: radial velocity histogram of ASCC 21. The cluster names, the medians of their radial velocities, and their errors are labeled on the diagram. It should be noted that in all radial velocities the diagram presents, the ratio of the radial velocities of both clusters to their errors is more than or equal to 3.

Further, to explore whether mass segregation occurs in our binary cluster, we adopted the minimum spanning tree method defined by Allison et al. (2009) to quantitatively investigate the mass segregation of these two clusters. Allison et al. (2009) defined the level of mass segregation as the “mass segregation ration” (Λ_{MSR}). This parameter greater than 1 indicates the signal of mass segregation in clusters. The method also was adopted by Zhang et al. (2020) to diagnose the mass segregation of Blanco 1. The Python code of the mass segregation we adopted in this work is available in the `gaia_oc_amd` repository published by van Groenigen et al. (2023) on GitHub¹. Figure 4 shows the Λ_{MSR} of ASCC 19 and ASCC 21. We found that ASCC 19 displays a faint signal of mass segregation but ASCC 21 not shows any signal. Combined with the above result that less massive member stars with large radial velocities are distributed

throughout the inner space of the binary cluster, this implies that the binary cluster is most likely undergoing a two-body relaxation process.

In addition, we analyzed in detail the outlier member stars with radial velocities exceeding $100 \text{ km}\cdot\text{s}^{-1}$ (colored triangles in the rightmost panel of Fig. 3), and the parameters of these stars are listed in Table 2. In our study, we found six outlier members with radial velocity over $100 \text{ km}\cdot\text{s}^{-1}$ in the binary cluster, of which four belong to ASCC 19, four belong to ASCC 21, and two belong to both ASCC 19 and ASCC 21. The parameters of the six stars can be seen in Table 2. It is well known that the rotation between the main star and the companion star in an eclipsing binary affects the intrinsic radial velocity of the eclipsing binary. Therefore, It is necessary to check whether these outlier members are eclipsing binaries.

We matched and obtained the data of five outlier member stars from the Transiting Exoplanet Survey Satellite (TESS) database. In order to determine whether these member stars are eclipsing binaries, first we plotted their lightcurves using the Python package `LightKurve` (Lightkurve Collaboration et al. 2018), then we extracted their frequencies using the `PERIOD04` software (Lenz & Breger 2005), and then we draw their phase diagrams, and finally we roughly determine their variable star types by periods, amplitudes, and effective temperatures.

Figure 5 presents the lightcurve and phase of TIC 264682835 that is one of these outlier members, with a radial velocity of $117.98 \pm 7.80 \text{ km}\cdot\text{s}^{-1}$. It is apparent that this star is a periodic variable star based on its period, which has ever been classified as BY Draconis-type variable star that belongs to rotational variables (Chen et al. 2020). Chen et al. (2020) pointed out that the rotational periods of BY Draconis-type variables range from 0.25 to 20 days. We found that the period of the object is about 1.5878 ± 0.0016 days which is within the range mentioned above, as shown in Fig. 5. Meanwhile, it is located at the lower edge of the main

¹ https://github.com/MGJvanGroenigen/gaia_oc_amd

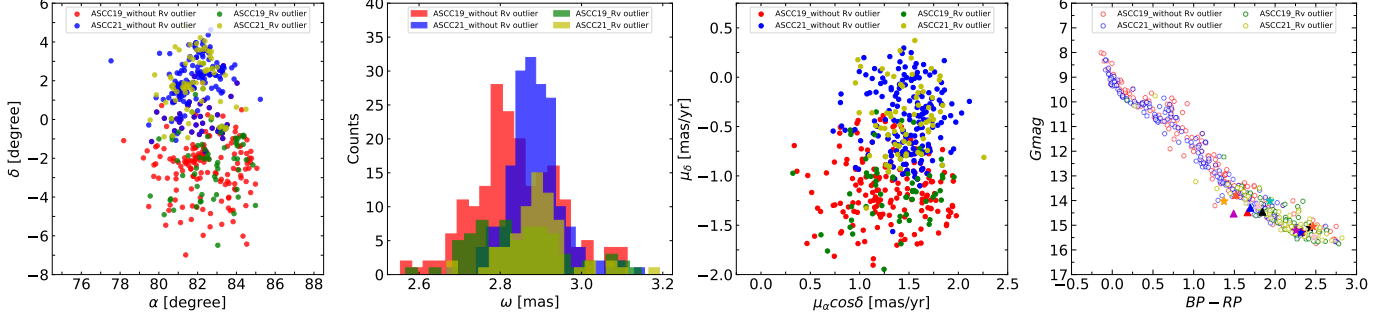


Figure 3. Distributions of members with a ratio of radial velocity to its error more than or equal to 3 of ASCC 19 and ASCC 21 in multi-dimensional parameter space. Leftmost panel: member distribution of both clusters in a 2D celestial coordinate system. Middle left panel: histograms of the member stars of both clusters in parallax space. Middle right panel: member distribution of both clusters in proper motion space. Rightmost panel: Color Magnitude Diagram (CMD) of the two clusters. The pentagrams of different colors represent member stars with outlier radial velocities, while triangles of different colors indicate member stars with outlier metal abundances. The various symbols and their meanings in all panels have been listed in the labels in the corresponding panels.

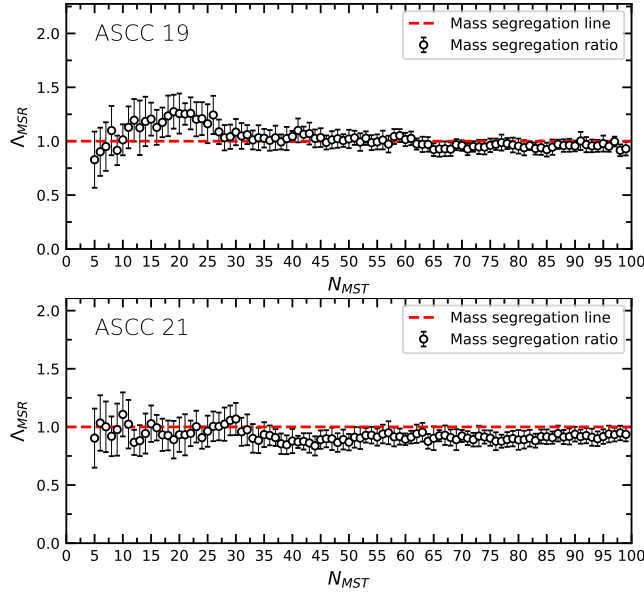


Figure 4. The “mass segregation ratio” (Λ_{MSR}) for ASCC 19 and ASCC 21. N_{MST} denotes the ordinal number of the member stars sorted by G-band magnitude, in sequence from bright to faint.

sequence in CMD of Fig. 3. Tsantaki et al. (2022) published its radial velocity $Rv = 20.418 \pm 0.921 \text{ km}\cdot\text{s}^{-1}$ and $T_{eff} = 3552.3 \pm 74.6\text{K}$ based on APOGEE data. In addition, Using Gaia BP/RP spectra, Verberne et al. (2024) provided its Rv of $302.009 \pm 290.928 \text{ km}\cdot\text{s}^{-1}$ and $T_{eff} = 3400 \text{ K}$. Since the radial velocity of the star is observed to be variable at different times, combined with its range of light variations as well as its effective temperature, therefore, we deduced that the star may be a binary star. So its radial velocity may not be its systemic radial velocity.

Similarly, we plotted the lightcurve and phase of TIC 264739961 that is one of these outlier members,

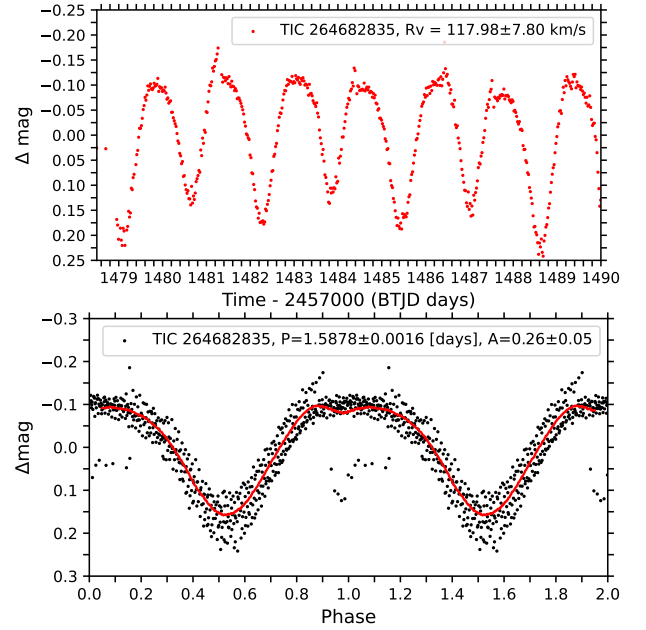


Figure 5. Upper panel: the lightcurve of TIC.264682835. Bottom panel: the phase diagram of TIC.264682835. The red curve represents the fitting curve to the phase. Its radial velocity, period, and amplitude have been labeled in the diagram.

with a radial velocity (Rv) of $137.78 \pm 5.76 \text{ km}\cdot\text{s}^{-1}$, as shown in Fig. 6. We found that this member is also a periodic variable star, with a period of 2.331 ± 0.025 days and amplitude of 0.013 ± 0.003 mag. Relying only on the star’s period and amplitude, we still cannot accurately determine its variable star type. Serna et al. (2021) also studied and classified it as a young star, with a projected rotational velocity of $23.3 \pm 0.8 \text{ km}\cdot\text{s}^{-1}$ based on Apache Point Observatory Galactic Evolution Experiment (APOGEE) data. Abdurro’uf et al. (2022) published its radial velocity $Rv = 39.20 \pm 0.08 \text{ km}\cdot\text{s}^{-1}$

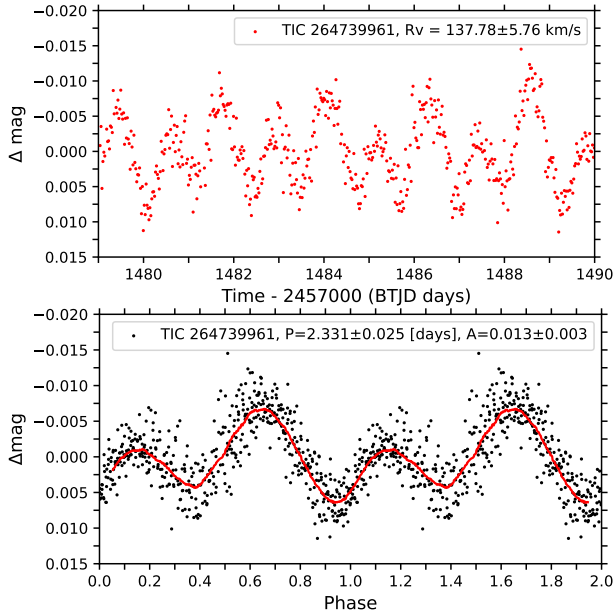


Figure 6. Upper panel: the lightcurve of TIC_264739961. Bottom panel: the phase diagram of TIC_264739961. All symbols are the same as that in Fig. 5

and effective temperature $T_{eff} = 3930.5$ K based on the seventeenth data release the Sloan Digital Sky Surveys (SDSS-DR17). In addition, there are its radial velocity $Rv = 24.1 \text{ km}\cdot\text{s}^{-1}$ (Ding et al. 2022), $Rv = 19.3 \pm 9.7 \text{ km}\cdot\text{s}^{-1}$ (Zhang et al. 2021), $T_{eff} = 3456$ K (Ding et al. 2022) based on the Large Sky Area Multi-Object Fiber Spectroscopic Telescope (LAMOST) data. Tsantaki et al. (2022) reported $Rv = 20.255 \pm 0.355 \text{ km}\cdot\text{s}^{-1}$, $T_{eff} = 3584.5 \pm 76.3$ K for the member based on APOGEE data. Although we can not determine its variable star type, it is expected that this member is likely a M-dwarf star, with the radial velocity consistent with that of its host cluster according to those parameters above and its location in CMD of Fig. 3.

Moreover, Figure 7 shows the light curves of three outlier stars (TIC 50788524, TIC 427451326, and TIC 50587538). We can roughly determine from this figure that these three outlier members are likely not eclipsing binaries because of their irregular light curves. For TIC 50788524, Gaia Collaboration et al. (2018) published its effective temperature $T_{eff} = 3668.05$ K, with Yu et al. (2023) and Verberne et al. (2024) reporting its $T_{eff} = 3532.1 \pm 102.0$ K and $Rv = 110.501 \pm 146.581 \text{ km}\cdot\text{s}^{-1}$, respectively. In addition, Abdurro'uf et al. (2022) also gave its Rv ($31.946 \pm 0.049 \text{ km}\cdot\text{s}^{-1}$, $18.038 \pm 0.067 \text{ km}\cdot\text{s}^{-1}$, and $20.059 \pm 0.065 \text{ km}\cdot\text{s}^{-1}$) and $T_{eff} = 3826$ K based on APOGEE data. According to these parameters above, we can not accurately determine its variable star type.

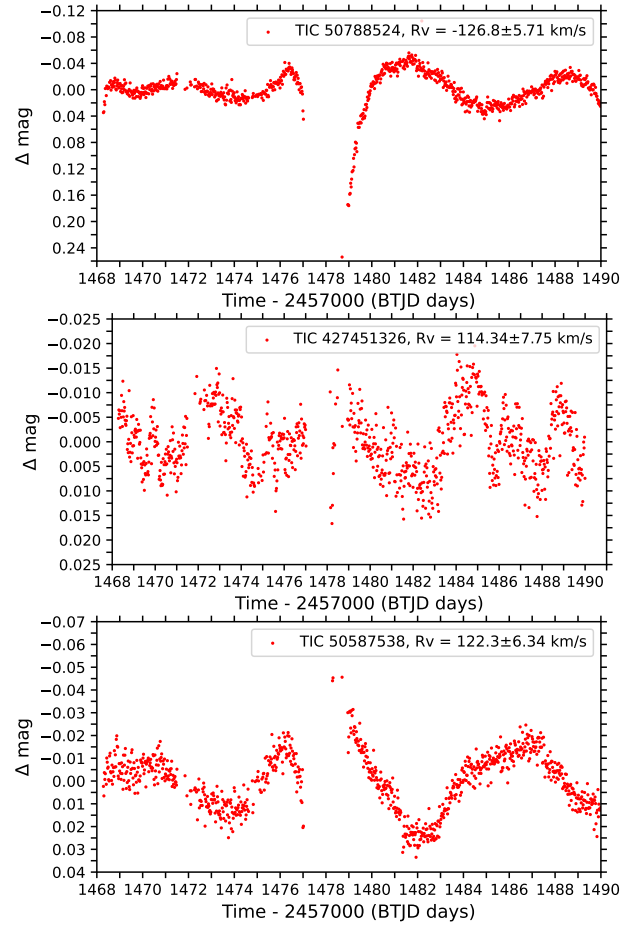


Figure 7. Upper panel: the light curve of TIC_50788524. Middle panel: the light curve of TIC_427451326. Bottom panel: the light curve of TIC_50587538.

However, we can infer from those parameters above that its Rv in this work may not be its systematic radial velocity, but its true Rv is likely still consistent with that of its host cluster. Similarly, TIC 427451326 was also studied by Abdurro'uf et al. (2022) who reported Rv of $-5.27 \pm 0.008 \text{ km}\cdot\text{s}^{-1}$, $43.74 \pm 0.06 \text{ km}\cdot\text{s}^{-1}$, $-4.03 \pm 0.05 \text{ km}\cdot\text{s}^{-1}$, $-5.61 \pm 0.06 \text{ km}\cdot\text{s}^{-1}$, and $43.63 \pm 0.07 \text{ km}\cdot\text{s}^{-1}$, with T_{eff} of 3924.6 K. Spina et al. (2021), Swiggum et al. (2021), and Tsantaki et al. (2022) published its Rv of $19.98 \text{ km}\cdot\text{s}^{-1}$, $20.11 \pm 0.02 \text{ km}\cdot\text{s}^{-1}$, and $19.97 \pm 0.30 \text{ km}\cdot\text{s}^{-1}$, respectively. They also gave its T_{eff} of 3730.0 ± 73.2 K. Obviously, like TIC 50788524, the systematic radial velocity of TIC 427451326 is likely consistent with the Rv of its cluster. Therefore, its Rv of $114.34 \pm 7.75 \text{ km}\cdot\text{s}^{-1}$ may not be its true Rv . In addition to these two stars, we can also find the T_{eff} and Rv parameters of TIC 50587538 from the literature. There are its T_{eff} of 3733.0 ± 122.0 K (Stassun et al. 2019) and 3387.2 K (Hernández et al. 2023) and Rv of -

$118.73 \pm 158.95 \text{ km}\cdot\text{s}^{-1}$ (Verberne et al. 2024). Due to the lack of the radial velocity of this star, we can not exclude the probability of its Rv in this work being its systematic Rv. If it is, it may be regarded as a star with high velocity, which means that its velocity may have been obtained during the two-body process. Further, this may also indicate that our binary cluster is undergoing a two-body relaxation process.

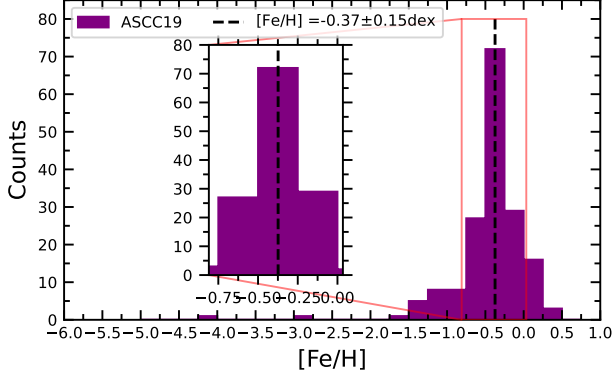


Figure 8. Histogram of the metallicity of member stars with a ratio of radial velocity to its error greater than and equal to 3 in ASCC 19.

3.3. Metallicity

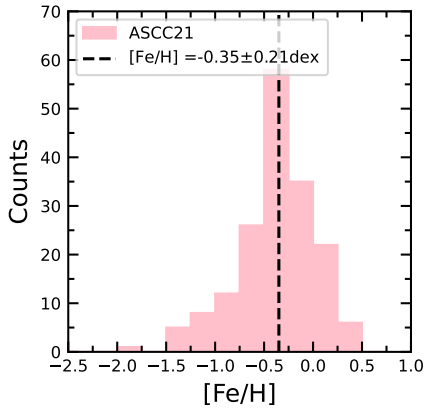


Figure 9. Histogram of the metallicity of member stars with a ratio of radial velocity to its error greater than and equal to 3 in ASCC 21.

The member stars of OCs are usually considered to have been born in the same molecular cloud and to have approximately the same metal abundance. In the case of binary clusters, if the two clusters have different metal abundances, then it can be shown that they were not born in the same molecular cloud. Conversely, the fact that they have the same metal abundance would indicate that they were born in the same molecular cloud, which would also indicate that they form a primordial binary

cluster. Following on from the previous subsection, I analyzed the metal abundances of all member stars with radial velocities and a ratio of radial velocities to their errors greater than three. Among these member stars, we obtained 171 member stars with metal abundance in ASCC 19 and 173 member stars with metal abundance in ASCC 21, respectively. We then plotted the histograms of the metallicity of ASCC 19 and ASCC 21, as shown in Figs. 8 and 9. For ASCC 19, its systematic metallicity ($[\text{Fe}/\text{H}]$) is about -0.37 ± 0.15 dex, with the $[\text{Fe}/\text{H}]$ of ASCC 21 being roughly -0.35 ± 0.21 dex, which was obtained by calculating their median and median error (MAD). It is obvious that the two clusters have the same metallicity, implying roughly their same ages, also see CMD in the rightmost panel of Fig. 3. Therefore, we can conclude that the binary cluster consisting of ASCC 19 and ASCC 21 is a primordial cluster pair.

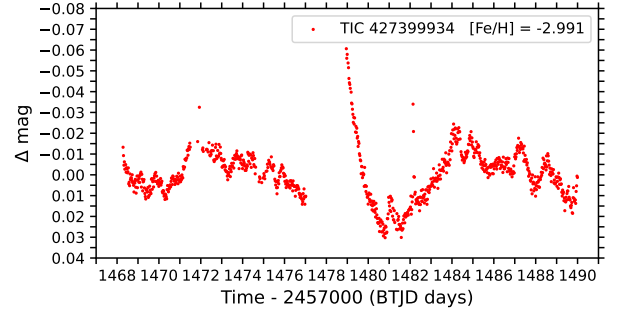


Figure 10. The lightcurve of TIC 427399934.

In addition, interestingly, there are two outlier members in the metallicity of ASCC 19, see their parameters in Table 2. We crossmatched and obtained TESS data for one star of them, which is TIC 427399934, with metallicity ($[\text{Fe}/\text{H}]$) of -2.991. Its irregular light curve is plotted in Fig. 10. From this figure, we can not determine its variable star type. Besides, Abdurro'uf et al. (2022) and Yu et al. (2023) published its $[\text{Fe}/\text{H}]$ of -0.1007 ± 0.0119 dex and -0.120 ± 0.070 dex, respectively. These two values are apparently different from its $[\text{Fe}/\text{H}]$ in this work where it is almost 30 times larger than the values of $[\text{Fe}/\text{H}]$ in Abdurro'uf et al. (2022) and Yu et al. (2023). We speculated thus that TIC 427399934 is a metal abundance anomaly star if the three parameters are right, which can be regarded as a candidate that is anomalous in terms of metal abundance. For another outlier member, its $[\text{Fe}/\text{H}]$ is about -4.096, as shown in Table 2. There is no metal abundance data for it in the literature. Therefore, we can assume that it is a metal abundance anomaly star.

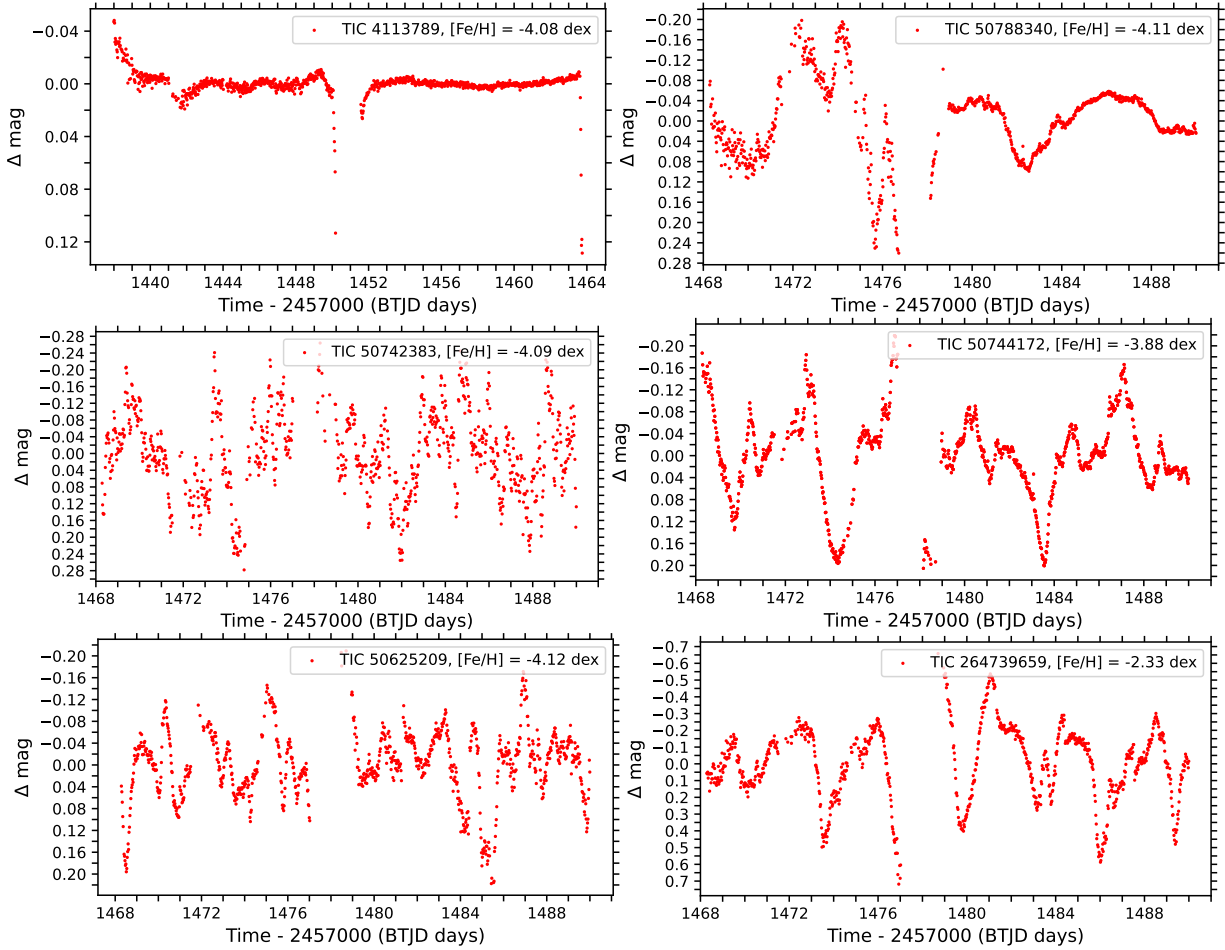


Figure 11. Upper left: the lightcurve of TIC 4113789; Upper right: the lightcurve of TIC 50788340; Middle left: the lightcurve of TIC 50742383; Middle right: the lightcurve of TIC 50744172; Bottom left: the lightcurve of TIC 50625209; Bottom right: the lightcurve of TIC 264739659.

Table 3. The parameters of outlier metallicity members

(1)	(2)	(3)	(4)	(5)	(6)	(7)
Gaia DR3 ID	Ra	Dec	[Fe/H]	TIC ID	Host cluster	Color in Figs. 3 and 12
–	(degree)	(degree)	(dex)	–	–	–
3210158170209393920	80.40	-4.89	-4.08	4113789	ASCC 19	Red triangle
3220694442244758784	83.11	-0.61	-4.11	50788340	ASCC 19 and ASCC 21	Pink triangle
3220661529910667904	82.83	-0.82	-4.09	50742383	ASCC 19 and ASCC 21	Purple triangle
3217634157789741952	83.03	-1.18	-3.88	50744172	ASCC 19	Black triangle
3220241585188156032	82.35	-1.42	-4.12	50625209	ASCC 19	Blue triangle
3223962504335346432	82.45	2.91	-2.33	264739659	ASCC 21	Coral triangle

Further, since the metallicities of ASCC 19 and ASCC 21 were acquired under the condition of limiting their members within the range of the ratio of $[\text{Fe}/\text{H}]$ to its error greater than and equal to 3. There thus may be a sample selection effect. In order to verify our conclusion of the cluster pair made up of ASCC 19 and ASCC 21 being a primordial binary cluster. We need

to check the metallicity of all members of the binary cluster. Figure 12 shows the distribution between the $[\text{Fe}/\text{H}]$ of all members with metallicity parameters and the distance to clusters' centers (three-dimensional centers) for them. How to obtain the distance parameters can be seen in Sec. 3.4. We found from Fig. 12 that both clusters are roughly composed of member stars

with three different metal abundances, as shown in the three bands from up to down in the left and right panels of the picture. This means that the formation of these two clusters may be the result of the merger of multiple subclusters. Meanwhile, this merger is well-mixed and homogeneous because the member stars of the three metal abundances are distributed in a penetrating pattern from the center of the two clusters to the periphery of the clusters, as shown in Fig. 12. This may be observational evidence that a cluster is formed from a hierarchy of subclusters. Although the members of ASCC19 and ASCC21 contain roughly three different metal abundances that are inconsistent with the preceding one above, their respective three metal abundances are roughly the same. Therefore, this confirms that our binary cluster is a primordial binary cluster.

Moreover, in Fig. 12, we found ten member stars with anomalous metal abundance. Among them, the two stars of ASCC 19 (orange and cyan pentagrams in the left panel) belong also to those with outlier radial velocities in Fig. 3 and Table 2. The rest include five members from ASCC 19 and three stars from ASCC 21 in which the two stars (pink and purple triangles in Fig.12) are not only the members of ASCC 19, but also the members of ASCC 21. The parameters of these stars are listed in Table 3. In addition, we also cross-matched these stars in the TESS database and obtained photometric data for a total of six stars. Based on the previous method, we plotted their light curves as shown in Fig.3. We found that these six stars have irregular light curves. Combining their locations in CMD of Fig. 3, we can determine that they are likely not binary stars.

In the case mentioned above, it is interesting to verify whether their metallicities are reliable and true. This may help us determine a sample candidate of stars with anomalous metal abundance in clusters, which provides observational evidence for the metal abundance evolution of clusters. Therefore, we referred to the metallicity parameters of the six stars from the literature. For TIC 4113789 (red triangle), Xiang et al. (2019) and Xiang et al. (2022) published its $[\text{Fe}/\text{H}]$ of -0.787 ± 0.059 dex and -0.367 dex based on LAMOST data, respectively, which is different from that of this work. So it may be not an outlier star in terms of $[\text{Fe}/\text{H}]$. We also found the metallicity parameters of TIC 50788340 (pink triangle) from the literature. They include $[\text{Fe}/\text{H}] = -0.573$ dex (Abdurro'uf et al. 2022), -0.678 dex (Abdurro'uf et al. 2022), 1.00 dex (Verberne et al. 2024), 0.01 dex (Román-Zúñiga et al. 2023), 0.006 dex (Sprague et al. 2022), -0.390 ± 0.080 dex (Yu et al. 2023), and -0.214 ± 0.016 dex (Tsantaki et al. 2022). These values still are not consistent with that

(-4.11 dex) of the star in this work. Apparently, it may be not the anomalous metallicity member. Following it, the metallicities of TIC 50742383 (purple triangle) were reported in literature as -2.00 dex (Jönsson et al. 2020), -2.50 dex (Abdurro'uf et al. 2022), 0.009 dex (Sprague et al. 2022), and -1.543 ± 0.028 dex (Tsantaki et al. 2022). We can conclude from these parameters that the member (purple triangle in Fig. 12) may be a truly anomalous metallicity star due to its being away from the metallicity of its host cluster. However, the rest three members are likely not the truly anomalous metallicity stars, such as TIC 50744172 (black triangle) of $[\text{Fe}/\text{H}] = -0.164 \pm 0.014$ dex (Jönsson et al. 2020), -0.500 dex (Jönsson et al. 2020), -1.011 dex (Abdurro'uf et al. 2022), -0.006 dex (Sprague et al. 2022), and -0.010 dex (Román-Zúñiga et al. 2023); TIC 50625209 (blue triangle) of $[\text{Fe}/\text{H}] = -0.505 \pm 0.015$ dex (Tsantaki et al. 2022), -0.636 ± 0.014 dex (Abdurro'uf et al. 2022), -0.892 dex (Abdurro'uf et al. 2022), -0.650 ± 0.090 dex (Yu et al. 2023), and 0.500 dex (Verberne et al. 2024); TIC 264739659 (coral triangle) of $[\text{Fe}/\text{H}] = -0.5$ dex (Jönsson et al. 2020), -0.616 ± 0.020 dex (Abdurro'uf et al. 2022), -0.883 dex (Abdurro'uf et al. 2022), -0.660 ± 0.120 dex (Yu et al. 2023), -0.606 dex (Wang et al. 2023), -0.653 dex (Fu et al. 2022), -1.000 dex (Verberne et al. 2024), and -0.094 dex (Sprague et al. 2022).

3.4. 3D Spatial Morphology

The study of the morphology of OCs may provide observational evidence for their formation and evolution (Hu et al. 2021a,b). Therefore, we would here make a diagnostic dynamical state for this binary cluster by investigating its morphology.

Since there are 191 member stars that are both members of ASCC 19 and ASCC 21, this suggests that the two clusters have crossed into each other in three dimensions. Therefore, here we investigated the 3D spatial structure of this binary cluster. Meanwhile, it is essential that combining with the tidal radii of the two clusters, we should roughly determine the dynamical state of the binary cluster. In order to get their tidal radii, we adopted the King model (King 1962) to fit their radial density profiles in 2D space, as shown in Fig. 13. The Python code we used in this work was developed by van Groeningen et al. (2023) and is also available in the `gaia_oc AMD` repository on GitHub mentioned above.

Then, we started to obtain the 3D projected distribution of the members of the binary cluster. We thus firstly calculated their 3D spatial coordinates within the helio-

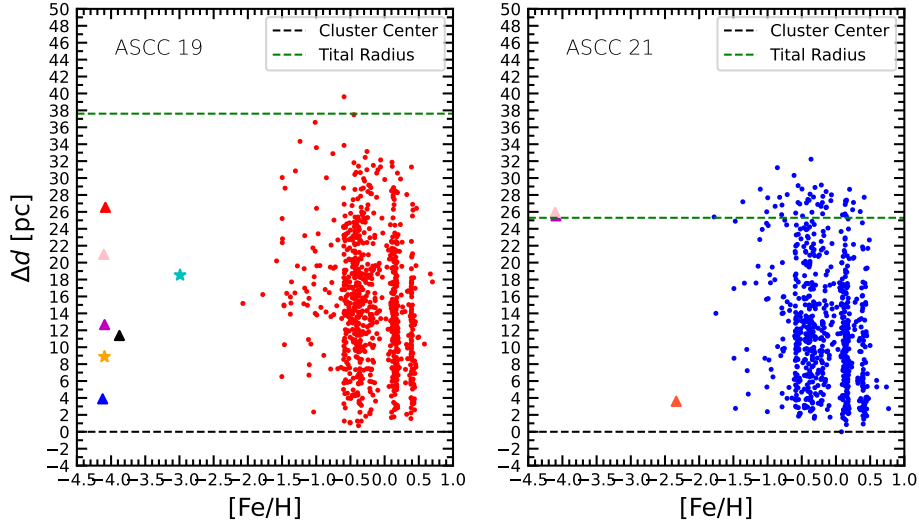


Figure 12. Left panel: the distribution (ASCC 19, red scatters) between the $[\text{Fe}/\text{H}]$ of all members with metallicity parameters and their distances (Δd) to clusters' centers (3D centers). The colored pentagams and triangles represent members with an anomalous metal abundance of ASCC 19. Right panel: the distribution (ASCC 21, blue scatters) between the $[\text{Fe}/\text{H}]$ of all members with metallicity parameters and their distances (Δd) to clusters' centers. The colored triangles represent members with anomalous metal abundance of ASCC 21. The black dashed lines in the diagram represent the 3D cluster centers of the two clusters, with their tidal radii being marked by the green dashed lines. The calculation of the tidal radii of the two clusters is detailed in Sec. 3.4.

centric Cartesian coordinate system (X , Y , and Z)². The coordinate calculation for each member of the pair was based on the `Python Astropy` package (Astropy Collaboration et al. 2013, 2018). However, because *Gaia*'s parallax has a symmetric error bar, direct inversion of the parallax leads to pseudo-stretching of the cluster's 3D morphology along the line-of-sight direction (see, e.g., Bailer-Jones 2015; Luri et al. 2018; Carrera et al. 2019). We so adopted a Bayesian distance correction model developed by (Carrera et al. 2019; Pang et al. 2021) and used by (Ye et al. 2021; Qin et al. 2023; Hu et al. 2023, 2024) to mitigate this problem. Eventually, we obtained the corrected distances of the members of ASCC 19 and ASCC 21 and further estimated their 3D spatial coordinates. Figure 14 shows the 3D projected morphologies of the binary cluster on the X - Y , Y - Z , and X - Z planes. We found that there is an overlap between the 3D projected distribution of the members of the two clusters, as well as their tidal circles. This may indicate a merger between ASCC 19 and ASCC 21.

Next, we fitted a 3D ellipsoid to the 3D spatial distribution of the member stars of ASCC 19 and ASCC 21, a method that has also been adopted by Hu et al. (2024).

Figure 15 displays the 3D spatial structure of this binary cluster, as well as the 3D fitting ellipsoids of its components. Like to the result in Fig. 14, there is also a crossover in their 3D fitting ellipsoids. In addition, we found that the distance between the centers of the fitted ellipsoids of ASCC 19 and ASCC 21 is approximately half the sum of their tidal radii. This also indicates that the pair may be undergoing a merger process.

3.5. Predicting Motion Trajectories

In order to verify whether ASCC 19 and ASCC 21 will merge into a cluster, we simulated their motion orbits using the `galpy.potential` module (`MWPotential2014`) within the `Python galpy` (Bovy 2015) package. It is an axisymmetric potential module that is composed of a Miyamoto-Nagai disc (Miyamoto & Nagai 1975), a bulge, and a dark matter halo modeled with a Navarro-Frenk-White (NFW) potential (Navarro et al. 1997). By inputting the position, parallax, proper motion, and radial velocity parameters of ASCC 19 and ASCC 21 into the module, we integrated the potential module and obtained the 3D spatial motion trajectories of these two clusters forward.

Figure 16 presents the projected motion trajectories of the two clusters on the X - Y (left), Y - Z (middle), and X - Z (right) planes within 400 Myr forward. We can see that this double cluster orbits roughly one and a half revolutions in the galactic disk within 400 Myr. They are now at the positions marked by black pentagram (ASCC 19) and triangle (ASCC 21) in the galactic

² The reference frame is an XYZ Cartesian coordinate system, with the Sun at its center. The positive X-axis is oriented from the Sun's projected position on the Galactic midplane towards the Galactic center, with the positive Y-axis aligning with the direction of the Galactic rotation. The positive Z-axis extends toward the north pole of the Galaxy.

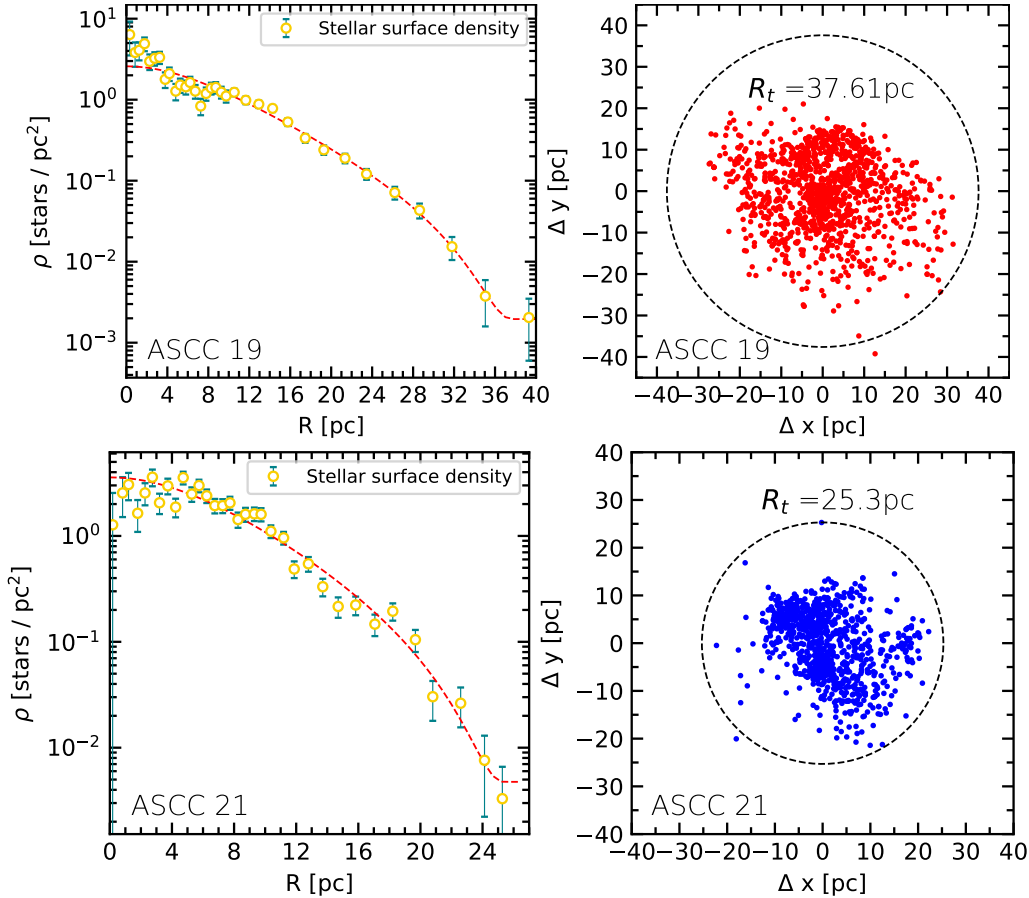


Figure 13. Upper left: the radial density profile of ASCC 19 fitted by King mode. Upper right: distribution of the members (red scatters) of ASCC 19 in two-dimensional space with its circle of tidal radius. Bottom left: the radial density profile of ASCC 21 fitted by King mode. Bottom right: distribution of the members (blue scatters) of ASCC 21 in two-dimensional space with its circle of tidal radius. The tidal radius of ASCC 19 is 37.61 pc, with the one of ASCC 21 being 25.30 pc.

disk. After 40 Myr, they will appear in the positions denoted by red pentagram (ASCC 19) and blue triangle (ASCC 21), as shown in Fig. 16. Therefore, it is possible that ASCC 19 and ASCC 21 will not merge a cluster as time passes based on this simulation for their motion orbits within galpy frame.

4. SUMMARY

Based on data from the literature, we discovered and confirmed for the first time that the combination of ASCC19 and ASCC21 is a physical binary cluster from the parameter spaces of 2D celestial coordinate system position, proper motion, parallax, and CMD. Meanwhile, Based on the analysis of its metal abundance, we are confident that it is a primary binary cluster.

In addition, obtaining photometric data from TESS, combined with parameters such as apparent velocities, effective temperatures, and so on, published in the literature, we then inspected its apparent velocity anomalies stars and found that a small number of them have real anomalous apparent velocities. This implies that this bi-

nary cluster may be undergoing a two-body relaxation process.

Next, we performed an in-depth analysis of the metal abundances in the binary cluster and found that the components in the binary cluster are all formed by deep homogeneous mixing of subclusters. In addition, we also found that there are obvious metal abundance anomalous stars in the binary cluster, however, from the photometry, as well as the metal abundance parameters that had been released in the literature, we are not sure if they are true metal abundance anomalies of the member stars, and simply consider them as a sample of possible metal abundance anomalies candidates.

Finally, we also performed a 3D morphological analysis of the binary cluster and found that there is a tendency for the components in the binary cluster to merge into a single cluster. However, based on our simulated orbital analysis of the components using galpy package, they will not merge into a cluster in the future but continue along similar orbits.

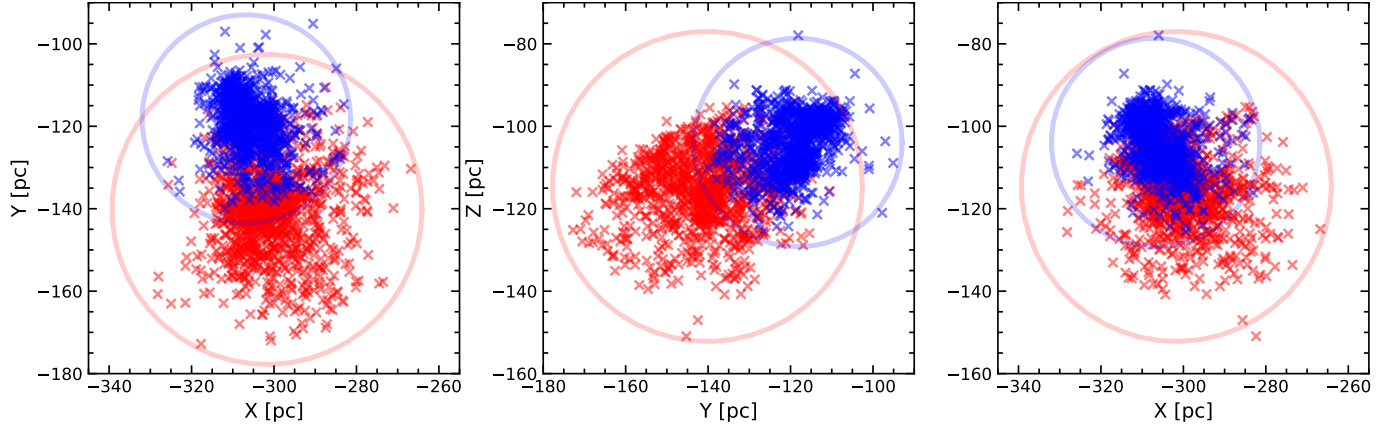


Figure 14. The three-dimensional (3D) projection distribution of the binary cluster on X-Y (left), Y-Z (middle), and X-Z (right) planes. The red and blue crosses indicate the members of ASCC 19 (tidal circle marked by red circle) and ASCC 21 (tidal circle marked by blue circle), respectively.

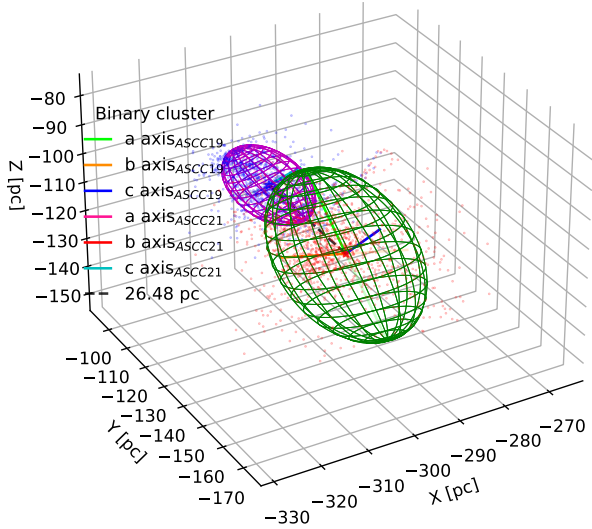


Figure 15. 3D spatial structure of the binary cluster (ASCC 19 and ASCC 21), with ellipsoidal curves. The green ellipsoid with its fitted center (red pentagram) denotes ASCC 19, with the purple ellipsoid with its fitted center (blue pentagram) marking ASCC 21. The small red and blue dots represent the members of ASCC 19 and ASCC 21, respectively. The black dashed line marks the distance between the fitted centers of the two clusters, with 26.48 pc. The different colored bars represent the different axes of the ellipsoids, respectively, as shown in the legend.

ACKNOWLEDGMENTS

This work is supported by the National Natural Science Foundation of China (NSFC) under grant xxx, the Fundamental Research Funds of China West Normal University (CWNU, No.xxx), the National Key R&D Program of China (Nos. xxx and xxx), the National Natural Science Foundation of China (NSFC) under grant xxx, the Chinese Space Station Telescope project: xxx, the Sichuan Youth Science and Technology Innovation Research Team (Grant No. xxx), and the Innovation Team Funds of China West Normal (No. xxx). Qingshun Hu would like to acknowledge the financial support provided by the China Scholarship Council program (Grant No. xxx). This study has made use of the Gaia DR2 and Gaia DR3, operated by the European Space Agency (ESA) space mission (Gaia). The Gaia archive website is <https://archives.esac.esa.int/gaia/>. The TESS data presented in this paper were obtained from the Mikulski Archive for Space Telescopes (MAST) at the Space Telescope Science Institute (STScI). STScI is operated by the Association of Universities for Research in Astronomy, Inc., under NASA contract NAS5-26555. The radial velocity, effective temperature, and metallicity parameters this work adopted are based on the data acquired through the Guoshoujing Telescope. Guoshoujing Telescope (the Large Sky Area Multi-Object Fiber Spectroscopic Telescope; LAMOST) is a National Major Scientific Project built by the Chinese Academy of Sciences. LAOMST is operated and managed by the National Astronomical Observatories, Chinese Academy of Sciences. Software: *Astropy* (Astropy Collaboration et al. 2018), *Galpy* (Bovy 2015), *LightKurve* (Lightkurve Collaboration et al. 2018), and *TOPCAT* (Taylor 2005).

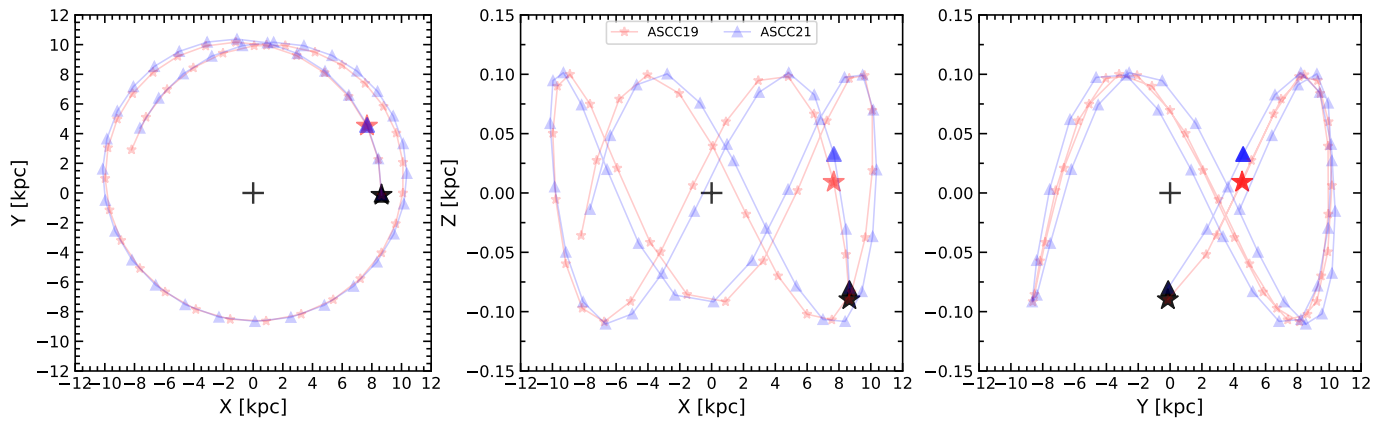


Figure 16. The 3D projected motion trajectories of ASCC 19 and ASCC 21 on the X-Y (left), Y-Z (middle), and X-Z (right) planes. The positions marked by black pentagram (ASCC 19) and triangle (ASCC 21) are now where they are, with their positions after 40 Myr being denoted by red pentagram (ASCC 19) and blue triangle (ASCC 21). The time span between two neighboring symbol marker points is 20 Myr for both red and blue trajectories.

REFERENCES

- Abdurro'uf, Accetta, K., Aerts, C., et al. 2022, *ApJS*, 259, 35.
- Allison, R. J., Goodwin, S. P., Parker, R. J., et al. 2009, *MNRAS*, 395, 1449.
- Astropy Collaboration, Price-Whelan, A. M., Sipőcz, B. M., et al. 2018, *AJ*, 156, 123.
- Astropy Collaboration, Robitaille, T. P., Tollerud, E. J., et al. 2013, *A&A*, 558, A33
- Bailer-Jones, C. A. L. 2015, *PASP*, 127, 994
- Bekki, K., Beasley, M. A., Forbes, D. A., et al. 2004, *ApJ*, 602, 730.
- Bergond, G., Leon, S., & Guibert, J. 2001, *A&A*, 377, 462.
- Bhatia, R. K. & Hatzidimitriou, D. 1988, *MNRAS*, 230, 215.
- Bica, E., Pavani, D. B., Bonatto, C. J., et al. 2019, *AJ*, 157, 12.
- Bovy, J. 2015, *ApJS*, 216, 29.
- Brown, J. H., Burkert, A., & Truran, J. W. 1995, *ApJ*, 440, 666.
- Carrera, R., Pasquato, M., Vallenari, A., et al. 2019, *A&A*, 627, A119
- Cantat-Gaudin, T., Jordi, C., Vallenari, A., et al. 2018, *A&A*, 618, A93.
- Cantat-Gaudin, T., Anders, F., Castro-Ginard, A., et al. 2020, *A&A*, 640, A1.
- Castro-Ginard, A., Jordi, C., Luri, X., et al. 2022, *A&A*, 661, A118.
- Casado, J. 2021, *Astronomy Reports*, 65, 755.
- Casado, J. 2021, *Research in Astronomy and Astrophysics*, 21, 117.
- Castro-Ginard, A., Jordi, C., Luri, X., et al. 2020, *A&A*, 635, A45.
- Chen, X., Wang, S., Deng, L., et al. 2020, *ApJS*, 249, 18.
- Conrad, C., Scholz, R.-D., Kharchenko, N. V., et al. 2017, *A&A*, 600, A106
- Chakrabarty, D. 2007, *A&A*, 467, 145.
- de La Fuente Marcos, R. & de La Fuente Marcos, C. 2009, *A&A*, 500, L13.
- Dehnen, W. 1998, *AJ*, 115, 2384.
- De Simone, R., Wu, X., & Tremaine, S. 2004, *MNRAS*, 350, 627.
- Dias, W. S., Alessi, B. S., Moitinho, A., et al. 2002, *A&A*, 389, 871.
- Ding, M.-Y., Shi, J.-R., Wu, Y., et al. 2022, *ApJS*, 260, 45.
- Evans, N. W. & Oh, S. 2022, *MNRAS*, 512, 3846.
- Famaey, B., Jorissen, A., Luri, X., et al. 2005, *A&A*, 430, 165.
- Fujimoto, M. & Kumai, Y. 1997, *AJ*, 113, 249.
- Fu, X., Bragaglia, A., Liu, C., et al. 2022, *A&A*, 668, A4.
- Gaia Collaboration, Brown, A. G. A., Vallenari, A., et al. 2018, *A&A*, 616, A1.
- Gaia Collaboration, Vallenari, A., Brown, A. G. A., et al. 2023, *A&A*, 674, A1.
- Goodwin, S. P. 1997, *MNRAS*, 284, 785.
- Hatzidimitriou, D. & Bhatia, R. K. 1990, *A&A*, 230, 11
- Hernández, J., Zamudio, L. F., Briceño, C., et al. 2023, *AJ*, 165, 205.
- Hu, Q., Zhang, Y., Esamdin, A., et al. 2021, *ApJ*, 912, 5
- Hu, Q., Zhang, Y., & Esamdin, A. 2021, *A&A*, 656, A49
- Hu, Q., Zhang, Y., Esamdin, A., et al. 2022, *ApJ*, 935, 142
- Hu, Q., Zhang, Y., Esamdin, A., et al. 2023, *A&A*, 672, A12
- Hu, Q., Zhang, Y., Qin, S., et al. 2024, *A&A*, 687, A291
- Hunt, E. L. & Reffert, S. 2023, *A&A*, 673, A114.
- Jönsson, H., Holtzman, J. A., Allende Prieto, C., et al. 2020, *AJ*, 160, 120.
- Kharchenko, N. V., Piskunov, A. E., Röser, S., et al. 2004, *Astronomische Nachrichten*, 325, 740.
- Kharchenko, N. V., Piskunov, A. E., Röser, S., et al. 2005, *A&A*, 440, 403.
- Kharchenko, N. V., Piskunov, A. E., Schilbach, E., et al. 2013, *A&A*, 558, A53
- King, I. 1962, *AJ*, 67, 471.
- Lada, C. J. & Lada, E. A. 2003, *ARA&A*, 41, 57.
- Lenz, P. & Breger, M. 2005, *Communications in Asteroseismology*, 146, 53.
- Li, Z. & Zhu, Z. 2024, *arXiv:2405.02530*.
- Lightkurve Collaboration, Cardoso, J. V. de M., Hedges, C., et al. 2018, *Astrophysics Source Code Library*. ascl:1812.013
- Liu, L. & Pang, X. 2019, *ApJS*, 245, 32.
- Luri, X., Brown, A. G. A., Sarro, L. M., et al. 2018, *A&A*, 616, A9
- Mamon, G. A., Cava, A., Biviano, A., et al. 2019, *A&A*, 631, A131.
- Mermilliod, J.-C. & Paunzen, E. 2003, *A&A*, 410, 511.
- Miyamoto, M. & Nagai, R. 1975, *PASJ*, 27, 533
- Navarro, J. F., Frenk, C. S., & White, S. D. M. 1997, *ApJ*, 490, 493.
- Noormohammadi, M., Khakian Ghomi, M., & Haghi, H. 2023, *MNRAS*, 523, 3538.
- Pang, X., Li, Y., Yu, Z., et al. 2021, *ApJ*, 912, 162
- Pavlovskaya, E. D. & Filippova, A. A. 1989, *Soviet Ast.*, 33, 6
- Portegies Zwart, S. F., McMillan, S. L. W., & Gieles, M. 2010, *ARA&A*, 48, 431.
- Pietrzynski, G. & Udalski, A. 2000, *AcA*, 50, 355.
- Qin, M. F., Zhang, Y., Liu, J., et al. 2023, *A&A*, 675, A67.

- Román-Zúñiga, C. G., Kounkel, M., Hernández, J., et al. 2023, *AJ*, 165, 51.
- Ryon, J. E., Gallagher, J. S., Smith, L. J., et al. 2017, *ApJ*, 841, 92.
- Serna, J., Hernandez, J., Kounkel, M., et al. 2021, *ApJ*, 923, 177.
- Song, F., Esamdin, A., Hu, Q., et al. 2022, *A&A*, 666, A75.
- Spina, L., Ting, Y.-S., De Silva, G. M., et al. 2021, *MNRAS*, 503, 3279.
- Sprague, D., Culhane, C., Kounkel, M., et al. 2022, *AJ*, 163, 152.
- Sim, G., Lee, S. H., Ann, H. B., et al. 2019, *Journal of Korean Astronomical Society*, 52, 145.
- Stassun, K. G., Oelkers, R. J., Paegert, M., et al. 2019, *AJ*, 158, 138.
- Subramaniam, A., Gorti, U., Sagar, R., et al. 1995, *A&A*, 302, 86
- Swiggum, C., D’Onghia, E., Alves, J., et al. 2021, *ApJ*, 917, 21.
- Taylor, M. B. 2005, *Astronomical Data Analysis Software and Systems XIV*, 347, 29
- Tsantaki, M., Pancino, E., Marrese, P., et al. 2022, *A&A*, 659, A95.
- van den Bergh, S. 1996, *ApJL*, 471, L31.
- van Groeningen, M. G. J., Castro-Ginard, A., Brown, A. G. A., et al. 2023, *A&A*, 675, A68.
- Verberne, S., Kuposov, S. E., Rossi, E. M., et al. 2024, *A&A*, 684, A29.
- Vesperini, E., McMillan, S. L. W., & Portegies Zwart, S. 2009, *ApJ*, 698, 615.
- Wang, R., Luo, A.-L., Zhang, S., et al. 2023, *ApJS*, 266, 40.
- Xiang, M., Ting, Y.-S., Rix, H.-W., et al. 2019, *ApJS*, 245, 34.
- Xiang, M., Rix, H.-W., Ting, Y.-S., et al. 2022, *A&A*, 662, A66.
- Ye, X., Zhao, J., Zhang, J., et al. 2021, *AJ*, 162, 171
- Yu, J., Khanna, S., Themessl, N., et al. 2023, *ApJS*, 264, 41.
- Zhang, Y., Tang, S.-Y., Chen, W. P., et al. 2020, *ApJ*, 889, 99.
- Zhang, L.-yun ., Meng, G., Long, L., et al. 2021, *ApJS*, 253, 19.